⋈USCAP

TECHNICAL REPORT

Co-staining of microRNAs and their target proteins by miRNA in situ hybridization and immunohistofluorescence on prostate cancer tissue microarrays

Markus Eckstein[1] · Verena Sailer[2,3] · Boye Schnack Nielsen[4] · Thomas Wittenberg[5] · Veit Wiesmann[5] · Verena Lieb[6] · Elke Nolte[6] · Arndt Hartmann[1] · Glen Kristiansen[2] · Nicolas Wernert[2] · Bernd Wullich[6] · Helge Taubert[6] · Sven Wach[6] · On behalf of the German Prostate Cancer Consortium (DPKK)

Abstract

The co-expression of miRNAs and their target proteins was studied on tissue microarrays from different prostate cancer (PCa) patients. PCa of primary Gleason pattern 4 (GP4), lymph node metastases of GP4, distant metastases, and normal tissue from the transitional and peripheral zones were co-stained by fluorescent miRNA in situ hybridization (miRisH) and protein immunohistofluorescence (IHF). The miRNAs and corresponding target proteins include the pairs miR-145/ERG, miR-143/uPAR, and miR-375/SEC23A. The fluorescence-stained and scanned tissue microarrays (TMAs) were evaluated by experienced uropathologists. The pair miR-145/ERG showed an exclusive staining for miR-145 in the nuclei of stromal cells, both in tumor and normal tissue, and for ERG in the cytoplasm with/without co-expression in the nucleus of tumor cells. The pair miR-143/uPAR revealed a clear distinction between miR-143 in the nuclei of stromal cells and uPAR staining in the cytoplasm of tumor cells. Metastases (lymph node and distant) however, showed tumor cells with cytoplasmic staining for miR-143/uPAR. In normal tissues, beside the nuclei of the stroma cells, gland cells could also express miR-143 and uPAR in the cytoplasm. miR-375 showed particular staining in the nucleoli of GP4 and metastatic samples, suggesting that nucleoli play a special role in sequestering proteins and miRNAs. Combined miRisH/IHF allows for the study of miRNA expression patterns and their target proteins at the single-cell level.

These authors contributed equally: Markus Eckstein, Verena Sailer.

Supplementary information The online version of this article (https://doi.org/10.1038/s41374-019-0251-8) contains supplementary material, which is available to authorized users.

✉ Helge Taubert
helge.taubert@uk-erlangen.de

[1]   Institute of Pathology, University Hospital Erlangen, FAU Erlangen-Nürnberg, Erlangen, Germany

[2]   Institute of Pathology, University Hospital Bonn, Bonn, Germany

[3]   Department of Pathology and Laboratory Medicine, Weill Cornell Medicine of Cornell University, New York, NY, USA

[4]   Bioneer A/S, Hørsholm, Denmark

[5]   Fraunhofer Institute for Integrated Circuits IIS, Erlangen, Germany

[6]   Department of Urology and Pediatric Urology, University Hospital Erlangen, FAU Erlangen-Nürnberg, Erlangen, Germany

Introduction

Prostate cancer (PCa) is the second most frequent tumor in men worldwide with ~1.1 million cases and 307,000 deaths per year [1]. Although there are well established clinical parameters of tumor stage [2] and tumor grade (e.g., Gleason grade [3]), there are no molecular biomarkers for diagnosis, prognosis and/or therapy monitoring or prediction that are clinically applied with a satisfactorily high specificity and sensitivity. The identification of molecular biomarkers as a comparison between normal prostate and PCa tissue is necessary, and their relation at the single cell level is desirable. Prostate anatomy is largely based on the work of McNeal [4, 5]. The normal prostate consists of five zones: the periurethral (mantle), transitional (5% of glandular prostate), anterior (non-glandular), central (25% of glandular prostate), and peripheral zone (70% of glandular prostate) [4–7]. The prostate glands are formed by two cell layers, the basal cells and the luminal gland cells. There are fibromuscular stroma cells located between the glands and

on the anterior surface of the prostate. Remarkably, the majority of prostate cancers originate in the peripheral zone (peripheral glands). PCa is histomorphologically characterized by the loss of basal cells and prominent nucleoli. Previously, we identified by RNA sequencing and array technology, three microRNAs, i.e. miR-143, miR-145, and miR-375, which are significantly altered in their expression between PCa and normal tissue. Both miR-143 and miR-145 are downregulated, and miR-375 is upregulated in PCa tissue compared to normal tissue [8, 9]. Furthermore, we could verify the target genes and proteins as plasminogen activator receptor/urokinase-type (PLAUR/uPAR), v-ETS avian erythroblastosis virus E26 oncogene homolog (ERG), and the *S. cerevisiae* homolog of SEC23A (SEC23A) for miR-143, miR-145, and miR-375, respectively [10, 11, 12]. However, a study of the expression of these miRNAs and their target genes in PCa and normal prostate tissue at the single cell level has not yet been performed. Therefore, we applied a combined miRNA in situ hybridization (miRisH) and immunohistofluorescence (IHF) technique [13] to detect miRNAs and their target proteins in PCa. In this study, we explored the technical applicability of this staining technique in combination with a digital image acquisition using a collection of Gleason pattern 4 (GP4) tumors, lymph nodes of GP4 tumors, and distant metastases, as well as in normal prostate tissues, including peripheral and transitional zone tissues.

Materials and methods

Material

PCa tissue microarrays (TMAs) were prepared on behalf of the German Prostate Cancer Consortium (DPKK). They comprised PCa and normal tissue samples of (i) primary GP4 (76 cores), (ii) lymph node metastasis of cases with primary tumor GP4 (87 cores), (iii) distant metastases (56 cores), normal transitional zone (47 cores), and normal peripheral zone (77 cores) that were collected at the Institute of Pathology University Hospital Bonn (Table 1). The normal tissue is tumor adjacent normal tissue from radical prostatectomies. But it was justified by pathological review that normal tissue did not contain PCa tissue. All patients gave written consent for this study. This research is in compliance with the Helsinki Declaration.

Chromogenic in situ hybridization (ISH)

Chromogenic miRNA ISH was performed essentially as described previously [14] using a Tecan Evo automated hybridization instrument (Tecan, Männedorf, Switzerland). The following steps were performed on 5 μm-thick sections:

Table 1 Overview: TMAs

No.	TMA	Tissue	microRNA	Protein	Cores
DPKK-3	104	GP4	miR-145	ERG	76
DPKK-4	119	Lymph node GP4	miR-145	ERG	87
DPKK-10	121	Distant metastasis	miR-145	ERG	56
DPKK-11	122	Normal transitional	miR-145	ERG	47
DPKK-12	123	Normal peripheral	miR-145	ERG	77
DPKK-13	104	GP4	miR-143	uPAR	76
DPKK-16	119	Lymph node GP4	miR-143	uPAR	87
DPKK-14	121	Distant metastasis	miR-143	uPAR	56
DPKK-2	122	Normal transitional	miR-143	uPAR	47
DPKK-15	123	Normal peripheral	miR-143	uPAR	77
DPKK-21	104	GP4	miR-375	SEC23A	76
DPKK-22	119	Lymph node GP4	miR-375	SEC23A	87
DPKK-23	121	Distant metastasis	miR-375	SEC23A	56
DPKK-24	122	Normal transitional	miR-375	SEC23A	47
DPKK-25	123	Normal peripheral	miR-375	SEC23A	77

predigestion with proteinase-K (10 μg/ml) at 37 °C for 8 min, prehybridization at 55 °C for 15 min, incubation with double-carboxyfluorescein (FAM)-labeled locked nucleic acid (LNA) probes (Exiqon, Vedbaek, Denmark) [15] for miR-143-3p (GAGCTACAGTGCTTCATCTCA; predicted RNA Tm, 85 °C), miR-145-5p (AGGGATTCCTGGG AAAACTGGAC; predicted RNA Tm, 84 °C), and miR-375 (TCACGCGAGCCGAACGAACAAA; predicted RNA Tm, 82 °C) at 20–40 nM in Exiqon hybridization buffer (Exiqon) for 2 h at 55 °C, stringent washes with saline–sodium-citrate (SSC) buffers, detection of the FAM-labeled probes with alkaline phosphatase-conjugated sheep anti-FAM Fab fragments (Roche, Basel, Switzerland), incubation with 4-nitro-blue tetrazolium and 5-brom-4-chloro-3′-Indolyl-phosphate substrate (Roche) for 1 h to allow the development of the dark-blue diformazan precipitate at the location of the bound probe, and finally, counterstaining with nuclear fast red. The slides were then dehydrated and mounted. The slides were processed in an AxioScan slide scanner (Zeiss, Oberkochen, Germany) and image acquisition was accomplished using the Zen software (Zeiss).

Double fluorescence staining

Combined miRNA ISH and IHC was performed as described elsewhere [13]. In brief, 5 μm-thick paraffin sections were deparaffinized using xylene and ethanol solutions. Sections were treated with proteinase-K at 10 μg/ml for 10 min at 37 °C. The sections were hybridized with the above-mentioned double-FAM-labeled LNA probes (miR-143 at 30 nM, miR-145 at 20 nM, and miR-375 at 40 nM) diluted in Exiqon hybridization buffer (Exiqon) and incubated at

55 °C for 2 h. The probes were detected with peroxidase-conjugated anti-FAM Fab fragments (Roche) followed by incubation with TSA-Cy5 substrate (Perkin Elmer, Waltham, MA, USA) for 7 min at room temperature. The slides were then washed in PBS and the miR-143-stained slides incubated with rabbit-anti-uPAR (generously provided by M. Illemann, Finsen Laboratory, Copenhagen, Denmark) at 3 μg/ml. The miR-145-stained slides were incubated with a rabbit monoclonal antibody against ERG (Clone ID: EPR3864; AbCam, Cambridge, UK) at 5 μg/ml and the miR-375-stained slides were incubated with a rat monoclonal antibody against SEC23A diluted 1:5 as described previously [10]. The antibodies were detected with Cy3-conjugated goat anti-rabbit or goat-anti-rat (Jackson Immunoresearch, West Grove, PA, USA). The sections were mounted with the DAPI-containing mounting medium, ProLong Gold (Thermo Fisher Scientific, Waltham, MA, USA). They were then evaluated and images were acquired using an AxioImager epifluorescence microscope (Zeiss) equipped with a ×20 objective and an HXP 120 V Illuminator with the following relevant filter sets (channels): Set 49/Dapi G365-BP445/50, Set 36-HE/FITC BP470/40-BP525/50, Set 43-HE/Cy3 BP550/25-BP605/70, and Set 50/Cy5 BP640/30-BP690/50. The exposure time was that of the auto-threshold determined by the Zeiss software for each of the four filter sets. Multiple-filter set acquisition also included the FITC channel to avoid image acquisition in areas with abundant autofluorescence signal present with varying intensity in the cores. Images were post-processed for balanced signal-to-noise using the AxioVision software (Zeiss).

Fluorescence image acquisition from scanned slides

Image acquisition was performed with an Axio Scan.Z1 epifluorescence whole slide scanner. The samples were illuminated by an HXP 120 V light source. The images were captured with an AxioCam MR R3 camera with a resolution of 1388 × 1040 pixels per tile. In combination with a Plan-Appochromat ×40/0.95 Korr M27 objective, this resulted in a pixel scaling of 0.163 μm × 0.163 μm. The excitation and emission light was filtered by a specific filter set for each single channel. We used the Zeiss filter set 49 for the DAPI channel, the Zeiss filter set 38 HE for GFP, the Zeiss filter set 43 HE for Cy 3, and the Zeiss filter set 50 for Cy 5. The scan procedure included several steps. First, all slides were inserted into individual slots into the whole slide scanner. Next, a preview image was taken of each slide. Based on these previews, an individual scan region covering all spots was manually selected for each tissue section. The scan process was conducted automatically for each slide, beginning by generating a focus map for the scan regions and finishing with the acquisition of the images. During the
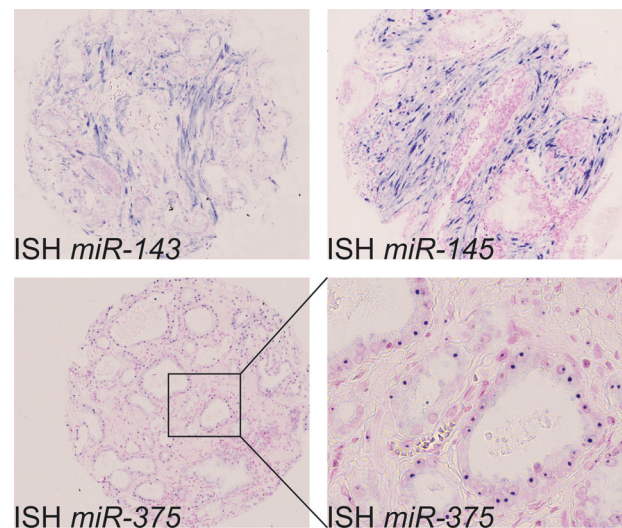
Fig. 1 Technical optimization of detection of miRNA by miRisH. Representative results of chromogenic miRisH on GP3 samples are shown

scan process ~106 tiles per tissue section were captured and stitched to one image for the scan region. After the scan process was completed, the slides were removed from the whole slide scanner. All image data was exported for further analysis as uncompressed tagged image file format (TIFF) images.
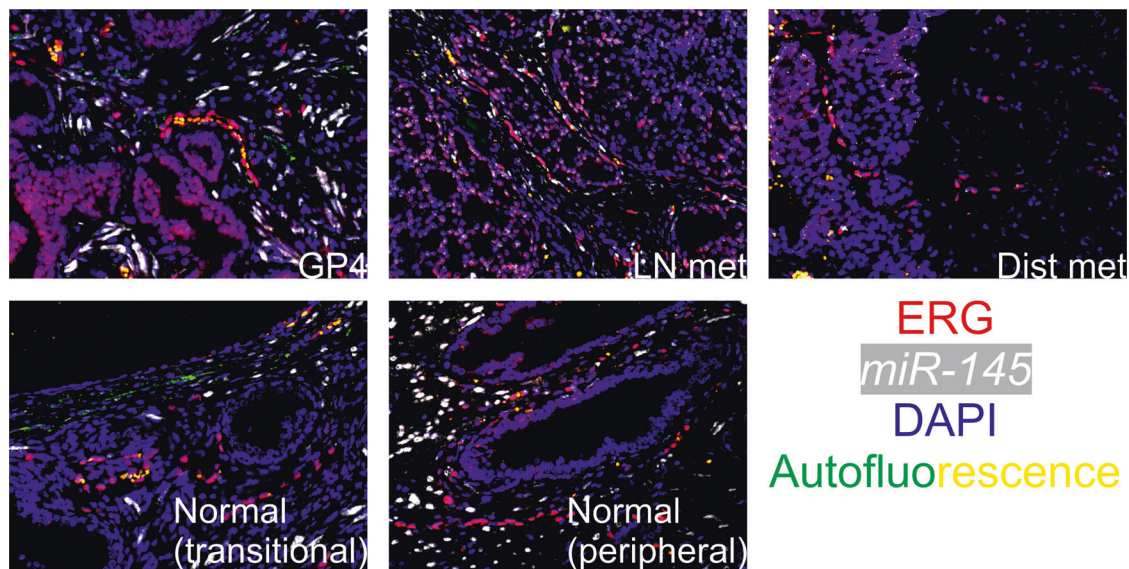
Results

TMAs of PCa tissue with GP4, lymph node metastases of GP4 tumors, distant metastasis, and normal tissue from the transitional and peripheral zones were studied (Table 1). First, the expression of the miRNAs was analyzed by bright field ISH (Fig. 1). This staining allowed visualization of the miRNA localization at the single-cell level. Remarkably, the localization of miR-375 was predominantly in the nucleoli of the tumor cells (luminal gland cells).

miR-145/ERG double fluorescence

In the GP4 and lymph node metastases (GP4) samples, miR-145 was expressed exclusively in the nucleus in the stroma cells but not in the tumor cells (Fig. 2; Table 2). However, the extent of staining was greater in the GP4 samples (2–90%) than in the lymph node samples (1–60%). In contrast, the ERG protein was not expressed in stromal cells, only in tumor cells, and was primarily cytoplasmic (71% and 61%); however, in some cases it was also found in the nucleus, both in the GP4 (43%) and in the lymph node samples (26%). Furthermore, ERG was most intensively stained in the endothelial cells and was considered as a positive control (Fig. 2).

Fig. 2 Detection of miR-145 and target protein ERG by fluorescence miRisH and IHF

Table 2 Overview: results miRish/IHF

miRNA/target protein	Tumor GP4		Metastasis		Normal (transitional and peripheral)	
	Stroma	Tumor cells	Stroma	Tumor cells	Stroma	Epithelial cells/gland cells
miR-145	Nuclei	Not	Few nuclei	Not	Nuclei	Not
ERG	Not	Nuclei/cytoplasm	Not	Few nuclei/cytoplasm	Not	Not (but endothel)
miR-143	Nuclei	Few cytoplasm	Few nuclei	Cytoplasm	Nuclei	Cytoplasm
uPAR	Not	Cytoplasm	(1 case cytoplasm)	Cytoplasm	(3 cases cytoplasm)	Cytoplasm
miR-375	Not	Nucleoli	Not	Nucleoli	Not	Only few cases weakly in nucleoli
SEC23A	n.a	n.a.	n.a.	n.a.	n.a.	n.a.

n.a. not applicable

Although distant metastases showed the same exclusive patterns of miR-145 being located only in stroma cells and ERG located only in tumor cells, both of these patterns occurred only in a few metastatic samples (Fig. 2; Table 2).

The stromal cells of the transitional zone and of the peripheral zone showed nuclear staining for miR-145, but a few normal gland cells also showed nuclear staining for miR-145. However, neither the stromal nor the gland cells of the transitional or the peripheral zone showed staining for ERG (excepting the endothelial cells) (Fig. 2).

miR-143/uPAR double fluorescence

In all GP4 samples, miR-143 was detected in the nucleus of stromal cells with four exceptional cases where tumor cells showed cytoplasmic miR-143 expression (Fig. 3; Table 2). The uPAR protein was not found in stromal cells, but in the cytoplasm of tumor cells and in intraductal macrophages, intravascular neutrophils, and endothelial cells. However, fibrotic tissue had uPAR-positive fibroblastic cells that co-localized with miR-143 (Fig. 3). These cells are most likely myofibroblastic cells.

In the lymph node metastasis and distant metastatic samples, miR-143 was mostly detected in the cytoplasm of tumor cells, but in some cases, it was also detected in the nucleus of stroma cells. The uPAR protein could be detected only in the cytoplasm in the tumor cells with one exceptional case (lymph node metastasis) where stromal cells showed staining for uPAR (Fig. 3; Table 2). However, only two cases (both lymph node and distant metastases) showed an exclusive pattern for miR-143 or uPAR in the tumor cells, i.e., the presence of both stains indicated co-expression in tumor cells.

The nuclei of stromal cells of the transitional and peripheral zones show miR-143 expression (Fig. 3; Table 2). However, the cytoplasm of gland cells also stained positive for miR-143 in the transitional zone and, in a few cases, in
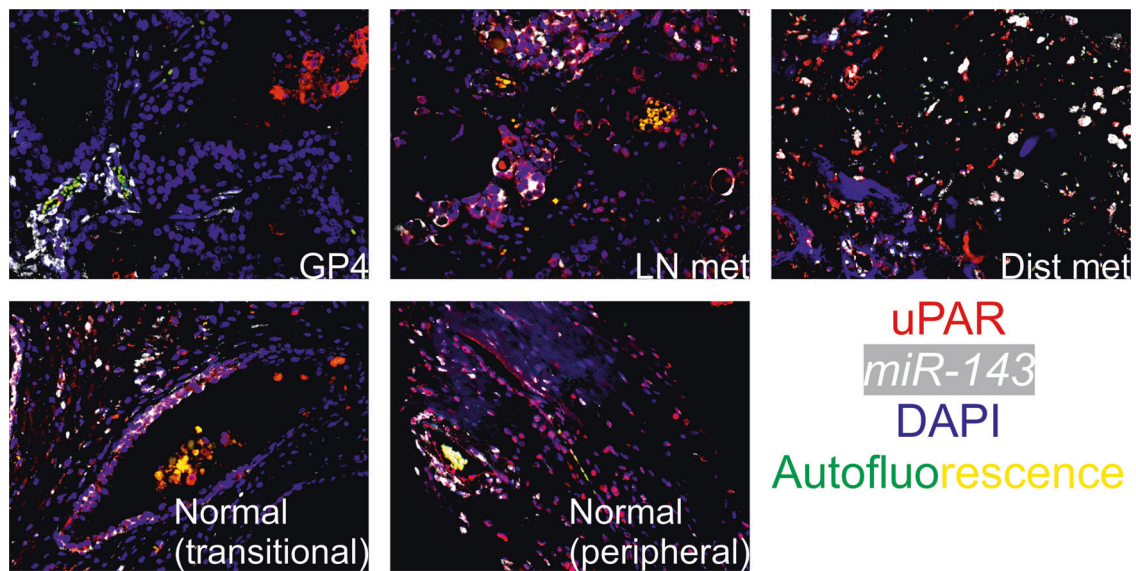
Fig. 3 Detection of miR-143 and target protein uPAR by fluorescence miRisH and IHF
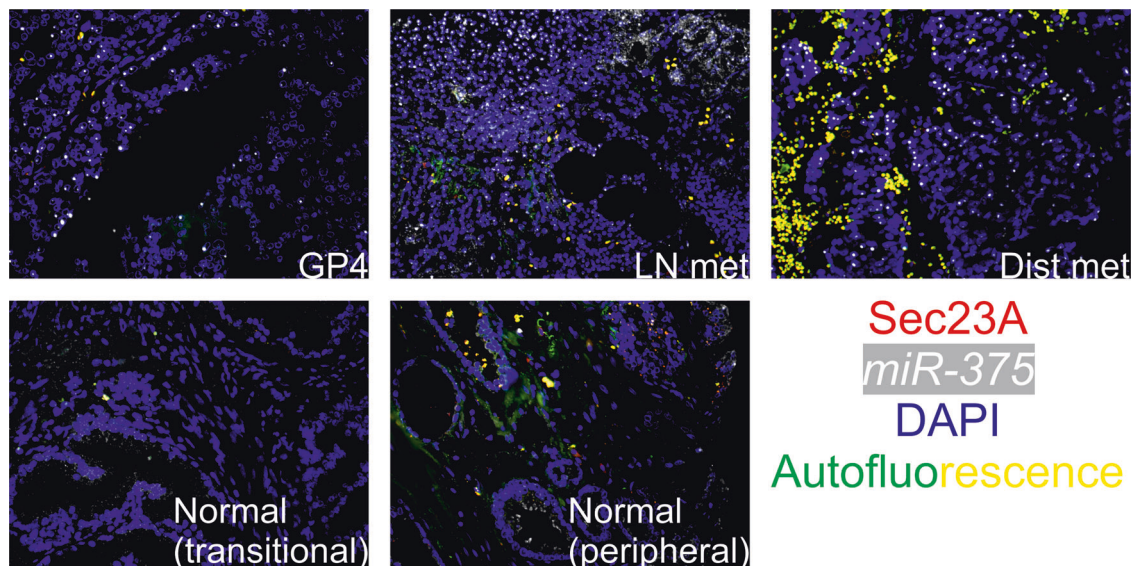
Fig. 4 Detection of miR-375 and target protein SEC23A by fluorescence miRisH and IHF

the peripheral zone. The uPAR protein was expressed in the cytoplasm of the gland cells and, as an exception, it was found in three cases in the stroma cells (transitional zone; Fig. 3). However, only one case showed an exclusive pattern for miR-143 or uPAR in the gland cells, i.e., the presence of both stains indicated co-expression in normal gland cells.

miR-375/SEC23A double fluorescence

The SEC23A antibody previously applied in Western hybridization [10] did not show specific staining in the FFPE material. Therefore, only miR-375 expression could be analyzed in the TMAs.

Remarkably, miR-375 was expressed in the nucleolus of the tumor cells in ~50% of the GP4 samples (Fig. 4; Table 2). Nearly all samples in the lymph node metastases of GP4 and half of the samples in the distant metastases expressed miR-375 in the nucleolus of the tumor cells (Fig. 4). The nucleoli of the normal luminal gland cells weakly expressed miR-375 in a few cases in the transitional zone and in the peripheral zone, respectively (Fig. 4).

Discussion

In this study, we applied a double fluorescence assay with paraffin samples combining LNA™-based microRNA ISH

and IHF, as previously described [13]. Here, we demonstrated its application using three different miRNAs, i.e. miR-143, miR-145, and miR-375 and their target proteins uPAR, ERG, and SEC23A, respectively. We have previously shown that miR-143 and 145 are downregulated, and miR-375 is upregulated in PCa tissue compared to normal tissue [9]. In addition, the proteins uPAR, ERG, and SEC23A could be verified as targets for miR-143, miR-145, and miR-375, respectively (Wach et al. unpublished data) [10, 11]. Here, we were interested to visualize the location of the miRNAs and their target proteins on the cellular level in tumor samples, i.e., tumor tissue of GP4, lymph node metastasis of GP4 cases and distant metastasis, as well as normal tissue samples from the transitional and the peripheral zone of the prostate.

As expected, in tumor tissue the pair miR-145 and ERG showed an exclusive staining pattern of miR-145 in the nuclei of stromal cells and ERG in the cytoplasm of tumor cells. In addition, miR-145 was seen in the stromal cells of the normal tissue samples, but no ERG staining was found except in endothelial cells, which is well established [16].

The pair miR-143 and uPAR showed a more varied picture. In the tumor tissue, the GP4 tissue showed a clear distinction between miR-143 in the nuclei of stromal cells and uPAR staining in a few tumor cells; however, the sample also contained fibroblastic cells that expressed both miR-143 and uPAR. In the lymph node and distant metastasis, fewer stromal cells showed staining for miR-143 in the nuclei, but tumor cells revealed cytoplasmic staining for miR-143. In addition, tumor cells showed cytoplasmic staining for uPAR; therefore, co-expression of miR-143 and uPAR was detected, and only a few cases showed exclusive staining for miR-143 or uPAR, which was generally expected. In the normal tissue, besides the nuclei of the stroma cells, gland cells could also express cytoplasmic miR-143, and uPAR staining was detected in the cytoplasm of gland cells. The exclusive staining of miR-143 and uPAR was rather exceptional in this experiment, and the detected co-expression was not expected.

Our results support the findings that miR-145 and miR-143 are predominantly detected in the stromal microenvironment, i.e., in mesenchymal cells, such as fibroblasts and smooth muscle cells, and not in epithelial tumor cells [17, 18]. Furthermore, the results indicate that it is important to study gene expression on the cellular level to avoid misinterpretations of results from analyses of mixed tissues and cell lines [18].

Our results show that although miR-145 and miR-143, that are arranged as a gene cluster on chromosome 5q32-q33, are co-transcribed and their stromal expression pattern is known [18–20] they can still show distinct expression patterns in PCa, metastatic, and normal cells. Both genes have common [19] yet different functions that can be seen

at the functional level in different target genes, e.g., in the Ras-MAPK pathway [18, 21].

miR-375 showed a very particular staining pattern, which was restricted to the nucleoli of tumor cells and has not been previously described. This staining pattern was observed in ~50% of GP4 and distant metastases samples and for nearly all lymph node metastasis samples in the tumor cells. In the literature, there are only a few miRNAs that have been detected in the nucleoli [22, 23], and these do not include miR-375. This finding is of special interest since an increased nucleoli size is a characteristic feature of PCa cells that is already present in the prostatic intraepithelial neoplasia (PIN) [24], but it is not yet known how this occurs. The nucleolus has well-known functions in ribosome biogenesis, but it is also suggested to be a cellular stress sensor [25]. It has been reported that ribosomal RNA shows an enhanced transcription upon the application of purified androgen receptor complexes in vitro [26] and that androgens and estrogens stimulate ribosome biogenesis in prostate and breast cancer cells [27]. On the other hand, studies on rats have shown that castration leads to the progressive disorganization of the nucleolus in prostate cells, which can be reversed by testosterone injection [28]. In line with this, treatment with testosterone can increase the nucleolar androgen receptor density in satellite cells and myonuclei [29]. Together, these findings suggest that the AR expression is associated with the ribosome biosynthesis occurring in the nucleoli, and could be phenotypically reflected by an increased size of the nucleoli. miRNAs located in the nucleolus are stably associated with the nucleolus and are less engaged with the RNA-induced silencing complex (RISC), which could be a way to sequester mature miRNAs [23]. The tumor suppressor protein TP53, e.g., which plays a major role in PCa [30], can be sequestered to the nucleoli after cellular stress [31, 32]. In line with this Kumazawa et al. suggest that the nucleolus works as a sensor that transduces the intracellular energy status (e.g. glucose starvation) into the cell cycle machinery (TP53 activation) [33]. The MDM2 protein that degrades TP53 is known to be sequestered in the nucleoli [34]. miR-375 that targets TP53 [35] appears to also be sequestered in the nucleoli, as shown in this study. A link between miR-375 and the AR has been described in the literature, where miR-375 expression downregulates AR expression and AR has been shown to be located in the nucleoli at least in rat oocytes [36, 37]. Taken together, these findings lead to the theory that, in addition to its role in ribosome biosynthesis, the nucleoli may have a special sequestration function in PCa.

We hypothesize that the TP53 pathway is a common element linking the studied miRNAs and their target proteins in
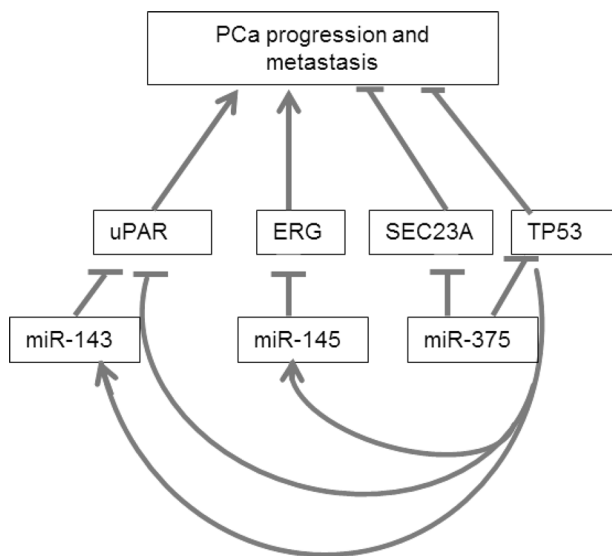
Fig. 5 Model: Association of the studied miRNAs and their target proteins in PCa progression and metastasis

PCa progression and metastasis (Fig. 5). The TP53 protein can activate miR143 and miR-145 transcription [38] but can inhibit uPAR activity by suppressing uPAR mRNA translation [39]. In turn, the uPAR protein can be regulated by miR-143 post-transcriptionally =[12]. However, the miR-375 that is overexpressed in PCa tissue [9] and in the serum of PCa patients [40] downregulates p53 expression [35].

In conclusion, we show the technical applicability of miRisH/IHF staining in combination with an automated digital image acquisition for larger sample collections.

Compliance with ethical standards

Conflict of interest The authors declare that they have no conflict of interest.

Publisher's note: Springer Nature remains neutral with regard to jurisdictional claims in published maps and institutional affiliations.

References

1. Ferlay J, Soerjomataram I, Dikshit R, et al. Cancer incidence and mortality worldwide: sources, methods and major patterns in GLOBOCAN 2012. Int J Cancer. 2015;136:E359–386.
2. Brierley JD, Gospodarowicz MK, Wittekind C, editors. Union for International Cancer Control (UICC): TNM classification of malignant tumors. 8th ed. Wiley-Blackwell, Oxford UK, Hoboken NJ; 2016.
3. Matoso A, Epstein JI. Grading of prostate cancer: past, present, and future. Curr Urol Rep. 2016;17:25.
4. McNeal JE. Regional morphology and pathology of the prostate. Am J Clin Pathol. 1968;49:347–57.
5. McNeal JE. The zonal anatomy of the prostate. Prostate. 1981;2: 35–49.
6. De Marzo AM, Platz EA, Sutcliffe S, et al. Inflammation in prostate carcinogenesis. Nat Rev Cancer. 2007;7:256–69.
7. Selman SH. The McNeal prostate: a review. Urology. 2011;78: 1224–8.
8. Szczyrba J, Löprich E, Wach S, et al. The microRNA profile of prostate carcinoma obtained by deep sequencing. Mol Cancer Res. 2010;8:529–38.
9. Wach S, Nolte E, Szczyrba J, et al. MicroRNA profiles of prostate carcinoma detected by multiplatform microRNA screening. Int J Cancer. 2012;130:611–21.
10. Szczyrba J, Nolte E, Wach S, et al. Downregulation of Sec23A protein by miRNA-375 in prostate carcinoma. Mol Cancer Res. 2011;9:791–800.
11. Hart M, Wach S, Nolte E, et al. The proto-oncogene ERG is a target of microRNA miR-145 in prostate cancer. FEBS J. 2013;280:2105–2016.
12. Wach S, Brandl M, Borchardt H, et al. Exploring the MIR143-UPAR Axis for the Inhibition of Human Prostate Cancer Cells In Vitro and In Vivo. Molecular Therapy - Nucleic Acids. 2019;16:272–283.
13. Nielsen BS, Holmstrøm K. Combined microRNA in situ hybridization and immunohistochemical detection of protein markers. Methods Mol Biol. 2013;986:353–65.
14. Nielsen BS, Jørgensen S, Fog JU, et al. High levels of microRNA-21 in the stroma of colorectal cancers predict short disease-free survival in stage II colon cancer patients. Clin Exp Metastasis. 2011;28:27–38.
15. Gould BR, Damgaard T, Nielsen BS. Chromogenic in situ hybridization methods for microRNA biomarker monitoring of drug safety and efficacy. Methods Mol Biol. 2017;1641:399–412.
16. Shaikhibrahim Z, Wernert N. ETS transcription factors and prostate cancer: the role of the family prototypeETS-1. Int J Oncol. 2012;40:1748–54.
17. Chivukula RR, Shi G, Acharya A, et al. An essential mesenchymal function for miR-143/145 in intestinal epithelial regeneration. Cell. 2014;157:1104–16.
18. Kent OA, McCall MN, Cornish TC, Halushka MK. Lessons from miR-143/145: the importance of cell-type localization of miRNAs. Nucleic Acids Res. 2014;42:7528–38.
19. Cordes KR, Sheehy NT, White MP, et al. miR-145 and miR-143 regulate smooth muscle cell fate and plasticity. Nature. 2009;460:705–10.
20. Goto Y, Kurozumi A, Enokida H, et al. Functional significance of aberrantly expressed microRNAs in prostate cancer. Int J Urol. 2015;22:242–52.
21. Santos JI, Teixeira AL, Dias F, et al. Restoring TGFβ1 pathway-related microRNAs: possible impact in metastatic prostate cancer development. Tumour Biol. 2014;35:6245–53.
22. Politz JC, Hogan EM, Pederson T. MicroRNAs with a nucleolar location. RNA. 2009;15:1705–15.
23. Li ZF, Liang YM, Lau PN, et al. Dynamic localisation of mature microRNAs in human nucleoli is influenced by exogenous genetic materials. PLoS One. 2013;8:e70869.
24. Brawer MK. Prostatic intraepithelial neoplasia: an overview. Rev Urol. 2005;7(Suppl 3):S11–18.
25. Olson MO. Sensing cellular stress: another new function for the nucleolus? Sci STKE 2004:pe10.
26. Mainwaring WI, Derry NS. Enhanced transcription of rRNA genes by purified androgen receptor complexes in vitro. J Steroid Biochem. 1983;19:101–8.
27. Ray S, Johnston R, Campbell DC, et al. Androgens and estrogens stimulate ribosome biogenesis in prostate and breast cancer cells in receptor dependent manner. Gene. 2013;526:46–53.

28. Dahl E. The ultrastructure of the accessory sex organs of the male rat. XI. Nuclear alterations of prostatic epithelial cells induced by castration. Cell Tissue Res. 1976;171:285–96.

29. Sinha-Hikim I, Taylor WE, Gonzalez-Cadavid NF, et al. Androgen receptor in human skeletal muscle and cultured muscle satellite cells: up-regulation by androgen treatment. J Clin Endocrinol Metab. 2004;89:5245–55.

30. Karanika S, Karantanos T, Li L, et al. DNA damage response and prostate cancer: defects, regulation and therapeutic implications. Oncogene. 2015;34:2815–22.

31. Wsierska-Gadek J, Horky M. How the nucleolar sequestration of p53 protein or its interplayers contributes to its (re)-activation. Ann N Y Acad Sci. 2003;1010:266–72.

32. Wesierska-Gadek J, Schloffer D, Kotala V, Horky M. Escape of p53 protein from E6-mediated degradation in HeLa cells after cisplatin therapy. Int J Cancer. 2002;101:128–36.

33. Kumazawa T, Nishimura K, Kuroda T, Ono W, Yamaguchi C, Katagiri N, et al. Yanagisawa Novel nucleolar pathway connecting intracellular energy status with p53 activation. J Biol Chem. 2011;286:20861–9.

34. Bernardi R, Scaglioni PP, Bergmann S, et al. PML regulates p53 stability by sequestering Mdm2 to the nucleolus. Nat Cell Biol. 2004;6:665–72.

35. Liu Y, Xing R, Zhang X, et al. miR-375 targets the p53 gene to regulate cellular response to ionizing radiation and etoposide in gastric cancer cells. DNA Repair. 2013;12: 741–50.

36. Östling P, Leivonen SK, Aakula A, et al. Systematic analysis of microRNAs targeting the androgen receptor in prostate cancer cells. Cancer Res. 2011;71:1956–67.

37. Szołtys M, Słomczyńska M, Duda M, Sakiewicz A, Otak A. Distribution of androgen receptor in rat ovarian follicles undergoing atresia at the beginning of pregnancy. Acta Histochem. 2005;107:357–64.

38. Zhang J, Sun Q, Zhang Z, et al. Loss of microRNA-143/145 disturbs cellular growth and apoptosis of human epithelial cancers by impairing the MDM2-p53 feedback loop. Oncogene. 2013;32: 61–69.

39. Shetty S, Velusamy T, Idell S, et al. Regulation of urokinase receptor expression byp53: novel role in stabilization of uPAR mRNA. Mol Cell Biol. 2007;27:5607–18.

40. Wach S, Al-Janabi O, Weigelt K, et al. The combined serum levels of miR-375 and urokinase plasminogen activator receptor are suggested as diagnostic and prognostic biomarkers in prostate cancer. Int J Cancer. 2015;137:1406–16.